THE JOURNAL OF PHYSICAL CHEMISTRY A

Article

pubs.acs.org/JPCA

Spectroscopic Properties of Benzene at the Air−Ice Interface: A Combined Experimental−Computational Approach

Rafał Kania,[†] Joseph K'Ekuboni Malongwe,[†] Dana Nachtigallová,*[,‡] Ján Krausko,[†,§] Ivan Gladich,[∥] Martina Roeselová,[‡] Dominik Heger,*[,†,§] and Petr Klán*[,†,§]

[†]RECETOX, Faculty of Science, Masaryk University, Kamenice 5, 625 00, Brno, Czech Republic

[‡]Institute of Organic Chemistry and Biochemistry, AS CR, v.v.i., Flemingovo nam. 2, 166 10 Prague, Czech Republic

[§]Department of Chemistry, Masaryk University, Kamenice 5, 625 00, Brno, Czech Republic

[∥]International School for Advanced Studies (SISSA), Via Bonomea 265, I-34136, Trieste, Italy

Supporting Information

ABSTRACT: A combined experimental and computational approach was used to study the spectroscopic properties of benzene at the ice−air interface at 253 and 77 K in comparison with its spectroscopic behavior in aqueous solutions. Benzene-contaminated ice samples were prepared either by shock-freezing of benzene aqueous solutions or by benzene vapor-deposition on pure ice grains and examined using UV diffuse reflectance and emission spectroscopies. Neither the absorption nor excitation nor emission spectra provided unambiguous evidence of benzene associates on the ice surface even at a higher surface coverage. Only a small increase in the fluorescence intensity in the region above 290 nm found experimentally might be associated with formation of benzene excimers perturbed by the interaction with the ice surface as shown by ADC(2) excited-state calculations. The benzene associates were found by MD simulations and ground-state DFT calculations, although not in the arrangement that corresponds to the excimer structures. Our experimental results clearly demonstrated that the energy of the $S_0 \rightarrow S_1$ electronic transition of benzene is not markedly affected by the phase change or the microenvironment at the ice−air interface and its absorption is limited to the wavelengths below 268 nm. Neither benzene interactions with the water molecules of ice nor the formation of dimers and microcrystals at the air−ice interface thus causes any substantial bathochromic shift in its absorption spectrum. Such a critical evaluation of the photophysical properties of organic contaminants of snow and ice is essential for predictions and modeling of chemical processes occurring in polar regions.

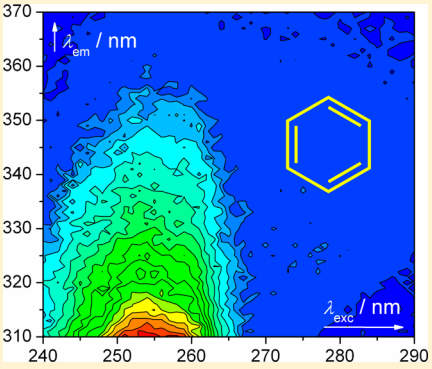

INTRODUCTION

At terrestrial temperatures, the surface of ice is a complex disordered system, which contains liquid or liquid-like compartments.[1,2] Its complexity increases when contaminant molecules are incorporated. The physicochemical properties of some organic molecules located at the air−ice interface have been studied by various experimental techniques, such as infrared, Raman,[3−6] absorption spectroscopy and mass and electron desorption spectroscopies,[7−17] or solvatochromic analysis,[18] to evaluate the extent of the contaminant−ice as well as contaminant−contaminant interactions. The magnitude of these interactions,[19−22] as well as the light absorption properties of the contaminants, can be influenced by temperature and the phase properties, and have a role in their (photo)chemical fate.[14−16,23−26]

The ice surface is susceptible to adsorption of gaseous molecules; the equilibrium partitioning at the air−ice interface is described by temperature-dependent energetics.[2] Most organic molecules cannot be incorporated within the ice lattice when their solutions are frozen; instead they are ejected to highly concentrated layers on the ice surface.[1,2] It has been demonstrated that shock-freezing of diluted aqueous solutions of aromatic compounds produced ice spheres (artificial snow) covered by ejected contaminant molecules, the major amount of which are in a direct contact with the gaseous reactants at the air−ice interface.[25,27,28]

Relatively high concentrations of various types of environmental pollutants, such as polycyclic aromatic hydrocarbons (PAHs), have been detected in polar and mountain areas far from regions of contaminant sources.[29,30] For example, concentrations of PAHs ranging from 0.1 to 10 ng kg^{-1} were reported from Summit, Greenland,[31] but they have also been found in urban snow.[23] The volatile and simplest aromatic hydrocarbon, benzene, has also been detected in the arctic atmosphere.[29,32] In general, PAHs are chromophores absorbing solar radiation, so they are predisposed to undergo various photochemical reactions. Therefore, the evaluation of their

Special Issue: Kenneth D. Jordan Festschrift

Received: January 30, 2014
Revised: June 19, 2014
Published: June 19, 2014

photophysical properties is essential to predict and model chemical processes occurring in polar regions.

Much effort has been made to reveal the nature of the benzene−water interactions in small clusters using the experimental methods, such as IR, resonant 2-photon ionization TOF MS, or UV hole-burning spectroscopies, and computational approaches.[33−40] The studies have revealed that the clusters possess a large degree of nonrigidity and structural variability. For example, Jordan and co-workers reported that the structures of the lowest energy[41] benzene−$(water)_8$ cluster conformers are cubic octamers of D_{2d} and S_4 symmetry.

The nature of the benzene−ice interactions has been investigated using impact electron spectroscopy, reflection−absorption infrared spectroscopy, and temperature programed desorption.[42] It was found that benzene is oriented parallel to the ice surface at low concentrations, and with an increased loading, the benzene molecules start to tilt leading eventually to the formation of 3-dimensional islands. Another study of the amorphous ice−benzene interactions using vibrational spectroscopy has revealed that the benzene molecules interact with the ice surface as proton acceptors which was evidenced by a downshifting of the ice dangling-H band.[43] It has been suggested that such a hydrogen bonding is responsible for binding of benzene to the water clusters. Several recent studies have indicated that the absorption properties of simple aromatic compounds are different in aqueous solutions and at the air−ice interface. Some of us have demonstrated that proton donating or accepting interactions between ice and the molecules of organic contaminants within aggregated contaminants, such as solvatochromic dyes, are larger than those in liquid solutions, as demonstrated by shifts in the contaminant absorption maxima upon freezing.[18] A small change in the absorption spectra of substituted aromatic compounds, such as phenol or anisole, in frozen aqueous solutions has also been observed.[16] The absorption spectra of simple aromatic compounds, such as benzene[14] or naphthalene[15] have been reported to exhibit bathochromic shifts at the air−ice interface. Several experimental as well as computational studies have demonstrated that aromatic compounds tend to associate on the ice surface,[13,15,17,25,27,42,44] even at loadings orders of magnitude below a monolayer coverage.[17]

In addition, computational simulations have recently been done to describe the properties of aromatic hydrocarbons, including benzene, at the ice-air interface.[17,44−47] These simulations provided evidence that individual molecules prefer a parallel alignment on the surface via the interactions of dangling O−H bonds and the delocalized aromatic π-electrons. The simulations performed using a grand-canonical Monte Carlo method have shown that these interactions determine the orientations of the adsorbates on the ice surface at lower pressures.[46] At higher concentrations, these adsorbates−ice interactions compete with interactions among the adsorbate molecules. In the case of naphthalene, it has been suggested using the molecular dynamics simulations that both the parallel and T-shape configurations mediated via $\pi-\pi$ stacking and CH−π interactions, respectively, contribute to the formation of self-associates on the ice surface.[13] These associates are weakly bound making their theoretical description computationally challenging even in the ground electronic state.

To model these associates in their electronically excited states, methods which properly describe the charge transfer processes, long-range electron correlations, and the higher polarizability of the excited state compared to the ground state have been developed. A number of computational studies have been performed to reveal the structure, stability and the character of interactions for benzene excimers.[48−57] It is now generally accepted that in the excimer the benzene molecules are arranged in a face-to-face sandwich orientation. Depending on the computational method, the distances between the center of masses of the two molecules are in the range of 0.295−0.315 nm,[48,49,52,55,56] which compares well with the experimentally observed distances of 0.300−0.350 nm.[58]

In this work, a combined experimental-computational approach was used to study the absorption and emission properties of benzene at the air−ice interface in comparison with its spectroscopic behavior in aqueous solutions. Various experimental techniques, such as UV absorption, diffuse reflectance and emission spectroscopies were utilized to examine the effects of the phase and microenvironment. Benzene self-organization and the formation of excited complexes were also spectroscopically evaluated. The character of the benzene−ice and benzene−benzene interactions in the ground and excited states was modeled by means of MD simulations and DFT calculations.

EXPERIMENTAL SECTION

Materials and Methods. Benzene (p. a., Sigma-Aldrich) was used as purchased. Water was purified on a Millipore Simplicity 185. Artificial snow[25] (ice spheres) samples were produced by spraying water droplets into a top-open insulated tank containing liquid nitrogen using a homemade nebulizing nozzle composed of a pair of 1 mm glass capillaries. The pressure of nitrogen flowing through the ejector capillary controlled the spraying rate and the grain size. The size of ice spheres, evaluated by an optical microscope, was in the 0.03−0.25 mm range,[25,26] slightly smaller than that previously reported for ice spheres produced by a hollow-cone brass nozzle nebulizer.[16,26,27] The samples were prepared by either shock-freezing (SF) or vapor-deposition (VD) techniques.[25] In the SF technique, benzene aqueous solutions of a known concentration were sprayed into liquid nitrogen using the nebulizer. VD was performed on pure (noncontaminated) artificial snow (30 g) placed in a glass desiccator kept at (253 ± 5) K inside a freezer[26] equipped with inlets to allow vapor circulation. While still in the same vessel, pure artificial snow was subjected to a slow (300 mL min^{-1}) flow of ambient air that passed through a test tube containing benzene (2 mL) for approximately 20 min. The artificial snow samples from both methods were stored over dry ice in a thermally insulated box prior to spectroscopic measurements to adjust the given temperature. For measurements at 77 K, freshly prepared artificial snow still in liquid nitrogen (SF method) was loaded into a cuvette and transferred into a liquid nitrogen-filled quartz Dewar vessel. For 253 K measurements, a dry ice frozen sample was allowed to gradually warm up in a thermo-controlled holder (for diffuse reflectance) or an Optistat (Oxford Instruments) cryostat (for fluorescence). Consistent absorbance and fluorescence spectroscopic properties were found no matter what type of preparation (SF or VD) was used. It is to be noted that the VD technique allowed producing samples of higher surface concentrations than those prepared using the SF method, in which the corresponding concentration was limited by the benzene water solubility. VD snow samples with very high benzene surface concentrations were prone to lose the deposited compound by sublimation (Figure S2 of the Supporting Information).

dx.doi.org/10.1021/jp501094n | J. Phys. Chem. A 2014, 118, 7535−7547

The absorption spectra were recorded on a Cary 5000i spectrometer (Agilent). The liquid samples were measured in 10 mm quartz cuvettes at ambient temperature of (295 ± 2) K. The transition energies are given in the format: (mean ± standard deviation) cm^{-1} (number of measurements, n). The diffuse reflectance spectra were recorded using an Agilent Praying Mantis Diffuse Reflectance (PM-DR) accessory equipped with a thermocell powder holder with quartz windows. The artificial snow sample was kept constant at the temperature as indicated. The holder was cooled by a mixture of dry ice and acetone. Each sample was equilibrated for 2 min prior to the measurements. The diffuse reflectance spectra did not change when the samples were kept at constant temperature for 20 min. The pure snow reference reflectance spectrum was used for the calculation of the remission (Kubelka–Munk) function, $f(R_\infty)$. The fluorescence measurements were performed on a perpendicular-geometry FLS 920 fluorescence spectrometer (Edinburgh Instruments) equipped with a 450 W Xe lamp and a PMT detector with double grating monochromators for both excitation and emission measurements. Fluorescence measurements were performed in standard 10 mm fluorescence cells. For measurements at 77 K, the sample cell was kept in a custom-made quartz Dewar vessel filled with liquid nitrogen. For measurements at 253 K, a prefrozen fluorescent cell was loaded with the ice sample and immediately transferred into an Optistat DN2 (Oxford Instruments) cryostat kept at (253.2 ± 0.1) K. For all measurements of emission spectra, the combination of a 10 nm excitation and 1 nm detection windows was used, while for the measurements of excitation spectra, 1 nm excitation and 10 nm detection windows were applied.

***Ab Initio* Calculations.** The structures of the benzene monomer and its complexes in the gas phase and their interactions with water molecules in the liquid phase and on an ice surface were optimized using density functional calculations employing the B97D[59] functional and the TZVP basis set.[60] The same approach was used to calculate the interaction energies of benzene with the ice surface. The reliability of this approach had already been tested by comparison of the interaction energies obtained with a more accurate DFT/CC scheme[61] for naphthalene dimer complexes and was successfully used for description of the interactions of 1-methylnaphthalene on ice surface.[17]

To describe benzene–water molecule interactions, several snapshots were taken from molecular dynamics trajectories (see below). All water molecules within the 0.9 nm distance from the center of mass of benzene were included in the cluster models used for subsequent *ab initio* calculations. The benzene complexes and all water molecules within the distance of 0.55 nm from the center of mass were optimized, while those at larger distances were kept intact.

Calculations of the monomer and dimer absorption spectra were performed at the ground-state optimized geometries using the second-order algebraic diagrammatic construction ADC(2)[62−64] with the resolution-of-identity method and the TZVP basis set. The ADC(2) method provided vertical excitation energies of benzene in reasonable agreement with more accurate methods (see the Results) and, at the same time, it is a computationally feasible method to study the spectra of large systems such as benzene dimers and their interactions with water molecules. The reliability of the TZVP basis set was tested by comparison of the excitation energies obtained with a more flexible def2-TZVP basis set of benzene clusters. The difference in the intermonomer separation calculated using TZVP and def2-TZVP was 0.002 nm, and the difference in the emission energy was 0.03 eV. The differences in the excitation energies of the first two excited states calculated with these two basis sets were less than 0.02 eV. Thus, the TZVP basis set was sufficient for the description of the relative energies of monomer and dimer species. To simulate the excited-state behavior of the benzene monomer and its dimers in water or on the ice surface upon light absorption, all water molecules within a distance of 0.55 nm from the solute center were included in these calculations. The number of molecules to mimic the solvent (e.g., 24 H_2O molecules in the case of solvated benzene) as well as ice surfaces was selected to keep the model extent computationally feasible and to model the solute environment at a comparable quality at the same time. For the spectral interpretations, the vibrationally resolved spectrum of benzene was calculated. These calculations were performed using the TD-DFT method[65,66] employing the B3-LYP functional[67] and TZVP basis set.

The emission spectra were calculated as the energy difference between the first singlet excited (S_1) and ground (S_0) states at the S_1 geometry minima. These minima were optimized at the ADC(2) level using a spin-component scaled approach[68] and the TZVP basis set. A Gaussian program package was used for the DFT calculations.[69] The ADC(2) calculations were carried out using a Turbomole program package.[70]

Molecular Dynamics Simulations. Molecular dynamics (MD) was used to sample the interfacial orientations and mutual arrangements of benzene molecules adsorbed at the surface of ice at 240 K, following the protocol that has been successfully utilized in our previous study.[17] The TIP5P-Ew model[71] was employed for water molecules, and the force field parameters for benzene were adopted from the GROMOS 53a6 all-atom force field.[72] A hexagonal I_h ice sample, consisting of 2880 water molecules, was constructed at 0 K using a Buch algorithm[73] to obtain an initial proton-disordered ice structure satisfying the Bernal-Fowler rules.[74] The dimensions of the initial ice sample were approximately 5.4 × 4.7 × 3.7 nm^3 in the x, y, z directions, respectively. The periodic boundary conditions were applied in all three dimensions. To equilibrate the ice to the target temperature, an NpT simulation of bulk ice at zero pressure was performed, in which the ice sample was first annealed by increasing the temperature from 0 to 240 K linearly over the course of 1.5 ns, and then equilibrating at 240 K for one additional ns. The pressure was controlled using the Parrinello–Rahman barostat[75] with a relaxation time of 2 ps and a compressibility of 10^{-7} bar^{-1}. Anisotropic pressure coupling was employed to allow all three sides of the simulation cell to fluctuate independently while the ice crystal lattice was heated to the target temperature. The pressure of the barostat was set to zero during the heating and equilibration in order to avoid any unwanted abrupt changes to the equilibrated ice crystal after the ice–vacuum interface was generated.[76]

A free ice surface was obtained by elongating the z-dimension of the simulation cell to 18 nm. In this way, an ice slab with two ice–vacuum interfaces was created in the middle of the simulation cell, with a layer of vacuum on both sides of the slab. The face exposed to vacuum was the basal (0001) plane. Two benzene molecules were placed on each of the ice slab surfaces, and a 30 ns NVT simulation was performed at 240 K. An initial 5 ns portion of the trajectory was discarded to account for the formation and equilibration of the disordered interfacial layer on the free basal plane; the remaining 25 ns were used to

dx.doi.org/10.1021/jp501094n | J. Phys. Chem. A 2014, 118, 7535−7547

sample the interfacial arrangements of the interacting benzene molecules adsorbed on ice. The system configurations were saved with a frequency of 1 ps; the selected snapshots were then extracted from the trajectory and used as the initial structures for subsequent *ab initio* calculations.

The MD simulations were carried out with the GROMACS (version 4.5.3) program package.[77] The leapfrog propagator[78] with a 1 fs time step was used for the integrating Newton's equations of motion. The canonical ensemble velocity–rescaling algorithm with a time constant of 0.1 ps was employed to control the temperature. A cutoff of 0.9 nm was applied to the Lennard-Jones potential and the real-space part of the Coulomb interactions. The long-range part of the electrostatic interaction was evaluated using the particle-mesh Ewald method[79,80] with a relative tolerance of 10^{-5}, a fourth order cubic interpolation, and a Fourier spacing parameter of 0.12. The C–H bonds were constrained using LINCS.[81] SETTLE[82] was used for constraining the geometry of the water molecules. The system configurations were saved with a frequency of 1 ps.

RESULTS AND DISCUSSION

Steady-State Absorption Spectroscopy. The absorption spectrum of benzene in aqueous solution ($c_{benzene}$ = 6.1 mM) at 295 K, as well as the diffuse reflectance spectra of benzene in artificial snow (SF; $c_{benzene}$ = 60 mM) and of frozen neat crushed benzene crystals, both at 253 K, are shown in Figure 1.

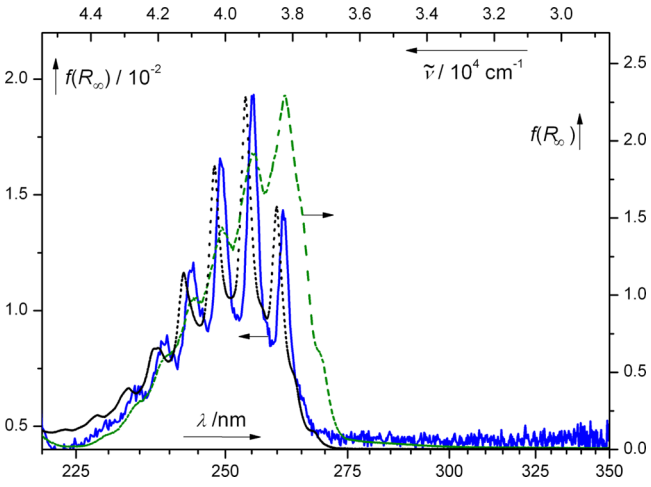

Figure 1. Remission (Kubelka–Munk) function, $f(R_\infty)$, of a benzene snow sample (c = 60 mM, 253 K, blue solid line, an SF method; left ordinate) and crushed frozen neat benzene diluted by silica (253 K, green dashed line, right ordinate). The absorption spectrum of a benzene aqueous solution (c = 6.1 mM, 295 K, black dotted line) is provided for the evaluation of the band positions. The absorbance values numerically agree with those on the right ordinate.

For SF samples, a nebulizer was used to spray very fine droplets into liquid nitrogen to produce ice spheres of a large specific surface area (~10^4 cm^2 g^{-1} as shown before[17]). The 60 mM benzene concentration used in these experiments was slightly above the monolayer coverage,[17] provided that all benzene molecules were ejected[25,27,28] to the ice grains surface during freezing. The concentration of benzene in the liquid samples was determined using a reported value of the molar absorption coefficient $\varepsilon_{254\ nm}$ = 188 M^{-1} cm^{-1} in aqueous solution.[83] The benzene absorption spectrum in water was in a good agreement with those reported previously.[14,83−85] The absorption spectrum of the lowest electronic transition $S_0 \rightarrow S_1$ ($1^1A_{1g} \rightarrow 1^1B_{2u}$) exhibited pronounced vibrational structure. We used a derivative analysis[86] to find that besides the major vibrational progression series (λ_{max} = 260.1, 253.9, 248.0, 242.5, 237.2, and 232.7 nm), there is a second vibrational progression series distinguishable as the inflection points in the absorption spectrum (λ_{max} = 263.6, 257.0, 250.9, 245.0, and 238.4 nm; Table 1, Figure S1).

The major vibrational series observed corresponded to the A_n^0 series, described for a liquid benzene spectrum,[84] which corresponds to the $6_0^1 1_0^n$ (n = 0–5) vibrational series identified in the gas phase[87] and calculated by Bernhardsson.[88] On the other hand, the minor vibrational progression has not been observed in the gas-phase benzene spectrum but can only be detected for the condensed phase due to symmetry reasons.[84] It has been assigned with the K symbol and corresponds to the 1_0^n (n = 0–4) vibrational transition. The K_1 band thus equals to the 0–0 transition. Our vibrational analysis of the spectra of benzene in aqueous solution matches the vibrations observed in liquid benzene[84] within experimental error, showing essentially no effect of the water microenvironment on these vibrational modes of benzene (Table S1). The longest wavelength band observed at 267 nm corresponded very accurately to a hot vibrational band (B_0^0, 6_1^0).[84,87] In the case of benzene aqueous solution, the average spacing of the vibrational progressions was found to be (928 ± 12) cm^{-1} (n = 4) and (1005 ± 85) cm^{-1} (n = 4) for the A and K series, respectively, determined for the first 4 values.

Two vibrational progression series of the $S_0 \rightarrow S_1$ ($^1A_{1g} \rightarrow {}^1B_{2u}$) electronic transition, calculated using the harmonic oscillator approximation and known experimental harmonic frequencies for the benzene 1^1B_{2u} excited state, are shown in Table 1 (the 0–0 energy was adjusted at 37922 cm^{-1}). The experimental values of the harmonic frequencies in the gas phase were used for the calculation of the K (1_0^n) and A ($6_0^1 1_0^n$) series in the 1^1B_{2u} excited state: 923 cm^{-1} for the first mode; 521 cm^{-1} for the sixth mode. The transition energy from the hot state was calculated by subtracting the value[88] of 608 cm^{-1} from that of the 0–0 energy level, which was the observed harmonic frequency of the sixth vibrational mode in the 1^1A_{1g} ground state of benzene. Both the experimental and predicted energy differences showed a perfect match, confirming the assignment of the vibrations.

The diffuse reflectance absorption spectrum of benzene in artificial snow (SF) at 253 K showed predominantly the A vibrational progression of the $1^1A_{1g} \rightarrow 1^1B_{2u}$ transition, bathochromically shifted by 1 nm compared to that in aqueous solution (Table 1). The average vibrational progression of the A series was found to be (872 ± 72) cm^{-1} (n = 6). The longest wavelength band still observable was found at 268.4 nm for SF samples, and it corresponds to the hot 6_1^0 transition.

To evaluate the impact of the benzene concentration and sample preparation method on the snow sample spectra, pure artificial snow was exposed to benzene vapors (VD) at 253 K to obtain as high benzene coverage as possible. Benzene sublimation progress was subsequently followed using diffuse reflectance spectroscopy (Figure S2). The spectra were dominated by the A vibrational series (resembling those observed in the aqueous solution, Table 1) with an average vibrational progression of (913 ± 126) cm^{-1} (n = 6). No concentration dependence on the shape and position of the bands was detected within 10 min (the spectrum acquisition

dx.doi.org/10.1021/jp501094n | J. Phys. Chem. A 2014, 118, 7535–7547

Table 1. Resolved Experimental and Calculated Maxima of the Vibrational Bands of the $S_0 \rightarrow S_1$ ($1^1A_{1g} \rightarrow 1^1B_{2u}$) Electronic Transitions of Benzene in a Different Microenvironment along with Their Assignments[a]

transition	band notation	λ_{max}^{abs}/nm (298 K)	λ_{max}^{DR}(SF)/nm (253 K)	λ_{max}^{exc}(SF)/nm (253 K)	λ_{max}^{exc}(VD)/nm (253 K)	λ_{max}^{DR}(s)/nm (253 K)	λ_{max}^{calc}/nm
6_1^0	B_0^0 (hot)	267.5		268.4	267.5	269.6	268.0
1_0^0	K_1 (0−0)	263.6	264.6	264.8		265.4	263.7
$6_0^1\,1_0^0$	A_0^0	260.1	261.2	261.2	259.3	261	260.1
1_0^1	K_2	257.0	258.2	257.2			257.4
$6_0^1\,1_0^1$	A_1^0	253.9	255.0	254.6	253.3	254.8	254.0
1_0^2	K_3	250.9	252.0	251.2			251.5
$6_0^1\,1_0^2$	A_2^0	248.0	249.0	248.6	247.3	249	248.2
1_0^3	K_4	245.0	246.0	245.4			245.8
$6_0^1\,1_0^3$	A_3^0	242.5	243.6	243.0	242.0	243.4	242.6
1_0^4	K_5	238.4		239			240.3
$6_0^1\,1_0^4$	A_4^0	237.2	239.0	238.0	237.5	238.4	237.3
1_0^5	K_6						235.1
$6_0^1\,1_0^5$	A_5^0	232.7	234.5	233.6	233.0	234	232.2
1_0^6	K_7			231.4	230.8		230.1
$6_0^1\,1_0^6$	A_6^0	227.8		228.6	227.0	229.4	227.4
1_0^7	K_8						225.3
$6_0^1\,1_0^7$	A_7^0			223.8			222.7

[a]abs: absorption; DR: diffuse reflectance; exc: excitation spectrum; SF: shock freezing; VD: vapor deposition; s: solid crystalline benzene; calc: calculated from known harmonic frequencies of the given mode using the harmonic oscillator approximation (see the text). A more intense *A* series is marked by the gray background.

time was less than 1 min with the acquisition rate of 450 nm min^{-1}). Neither broadening nor the shift of the bands of this vibrational series was observed for benzene concentrations corresponding to the emission intensities approximately 3 times higher than those attainable by SF of a saturated benzene solution.

In contrast, the spectrum of frozen (crystalline) benzene at 253 K displayed a marked absorption at the red edge of the spectrum that faded out at 275 nm. The analysis of the vibrational peaks showed that the longest wavelength band is the hot 6_1^0 transition and almost all signals can most likely be assigned to the *A* series (Table 1). All the bands were broader and bathochromically shifted by approximately 1 nm compared to those of aqueous solution. The mean vibrational progression of this *A* series was found to be (880 ± 55) cm^{-1} (n = 7).

Fluorescence. The normalized steady-state fluorescence emission and excitation spectra of artificial snow samples (c = 16 mM; 253 K; SF) are shown in Figure 2. The excitation at 248 nm resulted in fluorescence emission with a characteristic vibrational progression.[14,83,89−91] Clearly, the emission is dominated by the first mode of vibrational progressions in the ground state populated from the two states (0−0 and 6_0^1) of S_1. The normalized steady-state fluorescence emission and excitation spectra of a benzene aqueous solution (c = 1.4 mM; 295 K) are shown in Figure S4. The positions of the emission maxima (Table S2) for both samples were practically identical. However, an exact analysis of the emission spectra was not possible due to its complex vibrational pattern. Increased emission intensity above 290 nm in the case of a snow sample was the only apparent difference. We attempted to evaluate this difference by fitting Gaussian curves into the measured spectra (not shown); however, the fit was not unambiguous at wavelengths above 290 nm

The excitation spectrum of benzene in artificial snow (λ_{em} = 283 nm at 253 K; Figure 2) showed a better resolved vibrational progression compared to that of benzene aqueous solution (λ_{em} = 283 nm, 295 K, Figure S4). The mean vibrational progression of the *A* series was found to be (914 ± 66) cm^{-1} (n = 8) while that of the *K* series was found to be (1019 ± 98) cm^{-1} (n = 4). The 0−0 vibration was well resolved in the excitation spectrum of a snow sample as the K_1 band at 264.8 nm; the hot 6_1^0 band can also be observed at 268.4 nm. An apparent peak at 220 nm in the excitation spectra is most probably caused by the excitation light attenuation by a strong absorption below this wavelength.

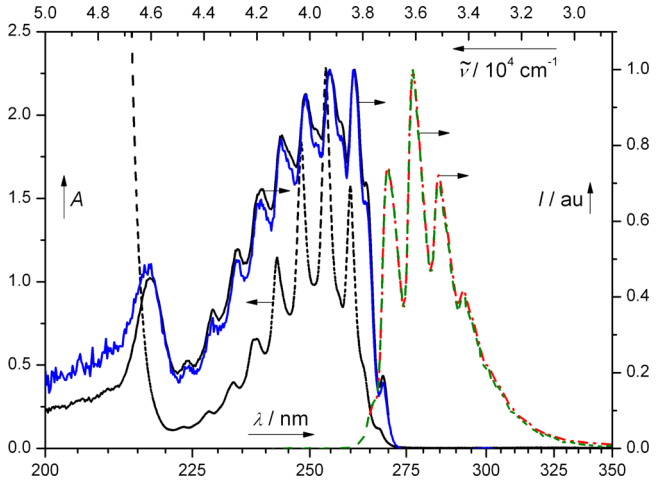

Figure 2. Normalized fluorescence excitation (283 nm, black solid line; 320 nm, blue solid line) and emission (243 nm, red dashed line; 214 nm, green dashed-dotted line) spectra of benzene in artificial snow sample (SF, 16 mM, 253 K). The absorption spectrum of benzene solution (6.1 mM, 295 K, black dotted line) is shown for comparison.

In order to disclose the presence of any distinctly absorbing dimer in the frozen samples, a series of the excitation spectra were recorded in the detection range of 280−320 nm at 77 K (Figure S6) and 253 K (Figure 2). However, no pronounced dependence of the excitation spectra on the selected detection wavelengths was found.

The fluorescence excitation and emission spectra of a benzene snow sample obtained at 77 K are shown in Figure S5. They exhibit the same features but are better resolved than

dx.doi.org/10.1021/jp501094n | J. Phys. Chem. A 2014, 118, 7535−7547

those measured at 253 K (Figure S4). The vibrational progressions were (915 ± 31) cm^{-1} (n = 4) and (1015 ± 91) cm^{-1} (n = 4) for the A and K series, respectively. The fluorescence excitation and emission spectra of benzene on artificial snow (vapor deposition) measured at 253 K also showed no bathochromic shift compared to the aqueous solution (Figure S7).

To probe the benzene absorption on the ice surface comprehensively, emission scans at the detection wavelengths of 310−400 nm with the excitation wavelengths in the 240−300 nm range were plotted in a 3D graph (Figure 3). This

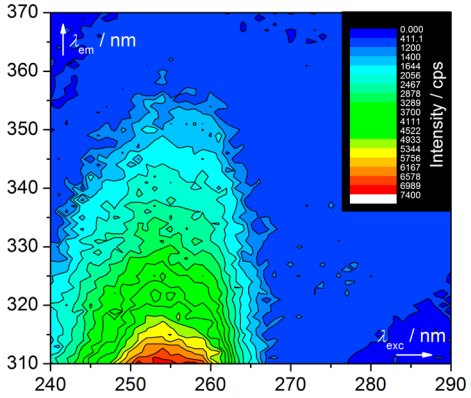

Figure 3. 3D plot of the emission scans (λ_{em} = 310−400 nm) as a function of the excitation wavelengths (λ_{exc} = 240−300 nm) for a benzene snow sample (c = 15.8 mM; 253 K; SF). The plot was corrected for a Raman scattering artifact by subtracting the 3D plot of pure artificial snow recorded with the same experimental parameters.

figure clearly demonstrated a total decline of the benzene emission for excitation wavelengths above 268 nm, apparent also in the absorbance and excitation spectra (Figures 1 and 2).

Computational Modeling of the Absorption and Emission Spectra of Benzene. The vertical excitation energies of the two lowest excited states, $S_0 \rightarrow S_1$ ($1^1A_{1g} \rightarrow 1^1B_{2u}$) and $S_0 \rightarrow S_2$ ($1^1A_{1g} \rightarrow 1^1B_{1u}$), of isolated benzene in vacuum and of benzene interacting with water molecules of water as a solvent or the ice surface (within the C_1 symmetry), calculated using the ADC(2) method, are given in Table 2. The energies calculated by previously used methods are also shown for comparison. Both the ADC(2) and the second-order approximate coupled cluster singles and doubles (CC2) methods overestimated the excitation energies by approximately 0.3 eV compared to the more accurate iterative approximate coupled cluster singles, doubles, and triples (CC3) and multireference complete active space perturbation (CASPT2) methods.

For the spectra interpretation, the vibrational progression of the $S_0 \rightarrow S_1$ electronic transition was calculated in vacuum at the B3LYP/TZVP level. Using this method, the energy difference between the lowest 0−0 and vertical transition energies was 0.259 eV, which is in good agreement with values obtained using the CASPT2[88] and coupled cluster singles and doubles CCSD[92] methods. This shift was then applied to obtain the lowest 0−0 transition energy at the ADC(2) level. The comparison between this value and the experimentally observed 0−0 transition energy of 262 nm[87] gave an energy difference of 0.230 eV. This value was used to shift all calculated vertical excitation energies (referred to in the text as

Table 2. Calculated Vertical Excitation Energies (E^{calc}) and Oscillator Strengths (f) of Benzene Monomer, and the Corrected Excitation Energies E^{corr} and Wavelengths λ^{corr} of the Corresponding Absorption Peaks for the Given Excited States

excited state	E^{calc}/eV[a]	f	literature data	E^{corr}/eV (λ^{corr}/nm)[b]
$S_1^{gas\ phase}$	5.247	0.000 00	4.84,[93] 5.27,[55] 5.19,[55] 5.06,[54] 5.08,[94] 5.06,[95] 5.04[96]	5.017 (247)
$S_2^{gas\ phase}$	6.621	0.000 00	6.30,[93] 6.68,[55] 6.74,[55] 6.68,[54] 6.54,[94] 6.22,[95] 5.97[96]	6.391 (194)
S_1^{water}	5.200	2×10^{-4}		
S_2^{water}	6.505	9×10^{-3}		
S_1^{ice}	5.263	9×10^{-5}		
S_2^{ice}	6.572	6×10^{-4}		

[a]Calculated with the ADC(2)/TZVP level on the geometries obtained at the B97D/TZP level. [b]Corrected by 0.230 eV to adjust the values according to the experimental data. The 0−0 transition energy was 4.952 eV, and the energy difference between the 0−0 and vertical transition energies was 0.295 eV.

E^{corr}) of benzene and its monomer to render the experimental and calculated energies comparable.

Modeling of the effect of water solvent on the absorption spectra of benzene has recently been investigated using the quantum mechanics/molecular mechanics studies and several DFT functionals.[97] It has been shown that relatively large clusters of water molecules are necessary to reach agreement with experiment. Employing the long-range corrected exchange-correlation density functionals ωB97X and ωB97X-D, red solvatochromic shifts of 0.03 and 0.02 eV, respectively, were found when compared to the values obtained in vacuum.

The first coordination shell, that is 24 water molecules, was used to calculate a solvatochromic shift in the absorption spectra of benzene. In agreement with the previous experimental[98] as well as computational[97] results, a small bathochromic shift of 0.047 eV, corresponding to a difference of 2 nm, was found in our calculations when we compared the $S_0 \rightarrow S_1$ transition energy of water-solvated benzene to that in vacuum. The oscillator strength of this transition was predicted to be much stronger in water compared to vacuum due to the perturbed symmetry. The corresponding excitation energy of benzene on the ice surface was found to increase by 0.06 eV compared to liquid water (i.e., a hypsochromic shift by 3 nm). A small decrease of the oscillator strengths was predicted when water solvent was exchanged by an ice surface. The red shift of the $S_0 \rightarrow S_2$ excitation energy upon transition from the gas phase to liquid water was calculated to be larger than that for $S_0 \rightarrow S_1$, although it was still marginal. It accounted for a decrease in the excitation energy by 0.116 eV, corresponding to a bathochromic shift of 3 nm. The transition from liquid water to ice surface resulted in a small increase (0.017 eV) in the $S_0 \rightarrow S_2$ excitation energy; thus, it predicted a hypsochromic shift of the absorption band by 2 nm.

To model aggregation of benzene on the ice surface, the excited-state calculations were performed for selected structures of benzene dimers found by the ground-state molecular dynamics simulations and subsequent optimization on the ice surface employing the B97D functional. Three situations were considered for these optimizations: two stable ground-state T-shaped dimer structures **B(S_0)-TS** (T-shaped) and **B(S_0)-TST** (T-shaped-tilted), as reported previously;[99−102] a third **B(S_0)-**

dx.doi.org/10.1021/jp501094n | J. Phys. Chem. A 2014, 118, 7535−7547

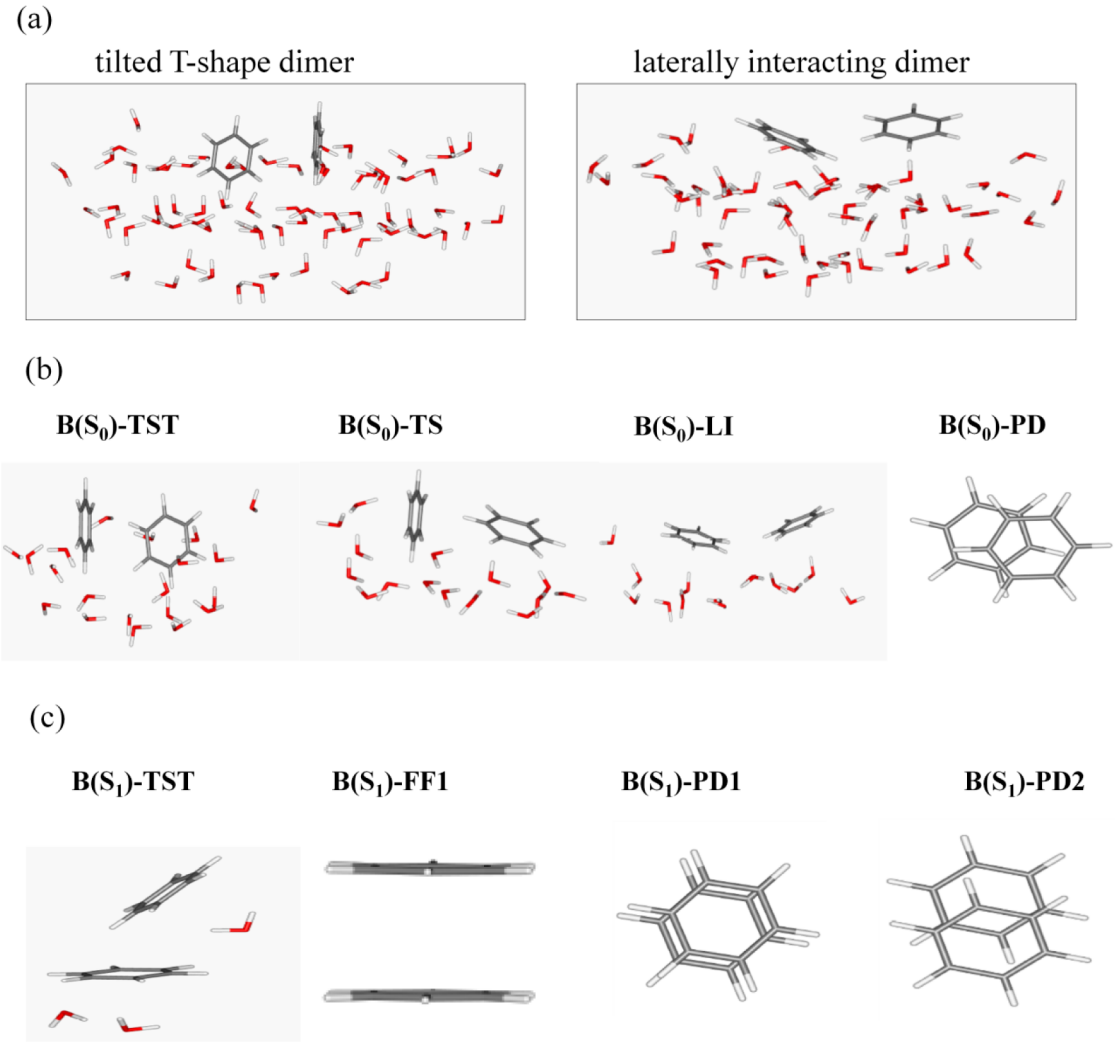

Figure 4. (a) Tilted T-shape and lateral arrangements of benzene molecules optimized on the ice surface. (b) Cluster models of benzene dimer associates on the ice surface and in the gas phase used for the calculations of the vertical excitation energies. (c) Optimized excited-state minima of tilted T-shape and face-to-face dimers, and parallel displaced structures perturbed from the face-to-face excimer by slides of 0.05 and 0.141 nm.

LI structure depicts the situation of two benzenes placed in a flat orientation on the ice surface and interacting laterally with each other (Figure 4). The clusters used for the optimization of tilted T-shape and laterally interacting dimers are shown in Figure 4a for illustration. The interaction energy of the benzene molecules was found to be −34 kJ mol^{-1}, which is in good agreement with the binding energy of 39 kJ mol^{-1} estimated from the temperature-programmed desorption experiment[42] performed for benzene interacting with amorphous solid water. This comparison assumes that the entropy does not change during the benzene association process because the ice surface is rigid. The interaction energies of the second benzene molecule were then −44 and −42 kJ mol^{-1} in laterally interacting and T-shape tilted complexes, respectively. The parallel-displaced structure, which is almost isoenergetic with the benzene dimers discussed above,[101,102] was not found on the ice surface during the time of molecular dynamics simulations. However, to compare the benzene absorption spectra in such a mutual orientation, the excited-state calculations of an optimized parallel-displaced structure in vacuum (**B(S_0)-PD**; Figure 4b) were also performed. The S_1 and S_2 state energies of the monomer and the four lowest excited states (S_1^d–S_4^d) of the dimer associates are listed in Table 3. The clusters of **B(S_0)-TS**, **B(S_0)-TST**, and **B(S_0)-LI** dimers located on the ice surface are shown in Figure 4b. The S_1^d and S_2^d states of the dimers were described by a linear combination of the S_1 states of the two monomers (Table 3). The next pair of the S_3^d and S_4^d states of the dimers is represented by a linear combination of the S_2 states of the monomers. To keep the comparison of the results consistent for various dimers, the gas-phase excitation energies were used; that is, the values for all three mutual orientations were obtained from the calculations after the water molecules were removed. The energies were lower by 0.230 eV, similarly to the shift calculated for monomer. In agreement with the previously reported data on the excitation energies of benzene associates,[53,84,103] a small bathochromic shift with respect to the monomer $S_0 \rightarrow S_1$ transition was found for all structural arrangements. On average, this decrease accounted for 0.026 and 0.013 eV for the S_1^d and S_2^d states, respectively. Similar results have also been obtained for a sandwich dimer structure using the CASPT2 method.[54] The inspection of the wave functions of the gas-phase dimers shows that the molecular orbitals of the **B(S_0)-TS** and **B(S_0)-TST** (Figure 4b) complexes involved in the excitations were mainly localized on one of the monomers with a small contribution of charge transfer between

dx.doi.org/10.1021/jp501094n | J. Phys. Chem. A 2014, 118, 7535−7547

Table 3. Corrected Vertical Excitation Energies (E^{corr})[a] and the Absorption Band Maxima (λ^{corr}) of Benzene Dimers Calculated for the Gas Phase[a]

structures[b]	E^{corr}/eV (λ^{corr}/nm)	
	S_1	S_2
monomer	5.017 (247) *0.016 (−1)*[c]	6.391 (194)

structures[b]	E^{corr}/eV (λ^{corr}/nm)			
	S_1[d]	S_2[d]	S_3[d]	S_4[d]
B(S_0)-TS	4.992 (248)	5.012 (247)	6.337 (196)	6.360 (195)
	0.008 (0)[c]	*0.018 (−1)*[c]	*−0.038 (1)*[c]	*−0.026 (1)*[c]
B(S_0)-TST	4.984 (249)	4.998 (248)	6.326 (196)	6.335 (196)
	0.015 (−1)[c]	*0.012 (−1)*[c]	*−0.034 (1)*[c]	*−0.022 (1)*[c]
B(S_0)-LI	5.001 (248)	5.003 (248)	6.373 (195)	6.381(194)
	0.032 (−2)[c]	*0.032 (−2)*[c]	*−0.026 (1)*[c]	*−0.014 (0)*[c]
B(S_0)-PD	4.989 (249)[d]	5.002 (248)[d]	6.322 (196)[d]	6.351 (195)[d]

[a]Calculated at the ADC(2)/TZVP level and corrected with the shift of 0.230 eV. [b]Optimized on the ice surface. [c]The shifts due to the interaction with the ice surface (ΔE ($\Delta\lambda$)) for the given excited states. [d]This structure was not found during the molecular dynamics simulations (see the text).

them. The water molecules present in the calculations of dimers on the ice surface caused delocalization of the wave functions in all cases, except in the case of **B(S_0)-LI**, where the excitation remained localized. Unlike in the cases of the above-mentioned associates, delocalized molecular orbitals were found for **B(S_0)-PD** in the gas phase. The decrease in the excitation energies (S_3[d] and S_4[d]) with respect to the S_2 state of the monomer was slightly larger compared to that of the S_1[d] and S_2[d] states; particularly, bathochromic shifts of 0.052 and 0.034 eV were found for the S_3[d] and S_4[d] states, respectively. The shifts in the excitation energies caused by the interaction of benzene and benzene dimers with the water molecules on the ice surface are also listed in Table 3. As in the case of monomer, interactions of benzene dimers with the water molecules on the ice surface caused only a negligible increase in the transition energies.

Optimization of benzene and the **B(S_0)-TST** (Figure 4b) dimer to the minimum of the S_1 state was performed in order to calculate the emission spectra of benzene associates. The resulting dimer structure **B(S_1)-TST** is shown in Figure 4c, and its vertical emission energy is given in Table 4. A small cluster, which includes the water molecules within the distance of 0.45 nm from the centers of benzene rings, was used for the dimer optimization. For the simulations of the emission spectra, we have considered the "limiting" case of the association, i.e., a benzene excimer characterized by the sandwich face-to-face arrangement of the two monomers (**B(S_1)-FF1**, Figure 4c). It is to be noted that this structure was not found during the ground-state dynamics simulations. As in the case of the absorption spectra calculations, the comparison was based on the gas-phase emission energies, i.e., obtained in the calculations after removing the water molecules from the **B(S_1)-TST** benzene−ice clusters (Figure 4c) optimized to the S_1 state. The calculated gas-phase emission $S_1 \rightarrow S_0$ energy of monomer was 4.906 eV ($\lambda^{calc} \sim 253$ nm); that is, it is hypsochromically shifted from the experimentally observed emission band by 0.187 eV (this value was used to adjust the calculated emission spectra).

Table 4. Corrected Gas-Phase Energies of the $S_1 \rightarrow S_0$ Transitions of Benzene Monomer and Dimers

structure	$\Delta E(S_1 \rightarrow S_0)$[a]/eV ($\Delta\lambda_{em}$/nm)
monomer	4.722 (263)
B(S_1)-TST	4.706 (263)
B(S_1)-FF1	3.850 (322)
B(S_1)-FF2[b]	4.014 (309)
B(S_1)-FF3[b]	4.342 (286)
B(S_1)-PD1[b]	4.016 (309)
B(S_1)-PD2[b]	4.732 (262)

[a]Calculated using ADC(2)/TZVP and corrected by 0.187 eV. [b]Perturbation from the minimal structure by increasing the intermolecular distance by 0.008 nm (**B(S_1)-FF2**) and 0.028 nm (**B(S_1)-FF3**) and by slide displacement of 0.050 nm (**B(S_1)-PD1**) and 0.141 nm (**B(S_1)-PD2**).

Rocha-Rinza and co-workers have performed a critical study on the reliability of the coupled cluster methods to describe the interactions in the benzene excimer.[55] These authors have shown that the CC2 method overestimates the binding energy of the complex, resulting in a minimum with a separation between the monomers of 0.286 nm, while more precise methods, such as CC3 and CASPT2 methods, give a value of 0.307 nm. The optimization employing the SCS-ADC(2) method used in our study gave an intermolecular distance of 0.299 nm (**B(S_1)-FF1**; Figure 4c) and an emission energy of 3.850 eV (after the adjustment by 0.187 eV was applied), corresponding to 322 nm. To estimate the effects of the mutual arrangement of two monomers on the emission energies, we performed additional calculations using an increased intermolecular distance between the two monomers or a small displacement between them. In the first case, an increase in the intermolecular separation to 0.307 nm (**B(S_1)-FF2**) and 0.327 nm (**B(S_1)-FF3**) provided emission energies of 4.014 and 4.342 eV, corresponding to the wavelengths of 309 and 286 nm, respectively. When two benzene molecules were displaced by 0.05 nm (**B(S_1)-PD1**) (Figure 4c), the emission energy was 4.016 eV, corresponding to 309 nm. At 0.141 nm (**B(S_1)-PD2**, Figure 4c), the emission band already overlapped with that of monomer. Thus, a band in the region of 310−320 nm should be anticipated in the emission spectra providing that an ideal face-to-face structure is present. The associates slightly perturbed by the ice surface should emit in the region of 290−310 nm. The T-shape structures did not provide any energy shifts from that of monomer.

Interpretation. Our spectroscopic as well as computational analysis demonstrates that the energy of the lowest singlet $S_0 \rightarrow S_1$ transition of benzene is practically unchanged by the water/ice surface microenvironment when compared to that obtained in the gas phase. Only marginal bathochromic shifts for the *A* series of the vibrational bands of benzene of (147 ± 11) cm^{-1} ($n = 5$) and (160 ± 23) cm^{-1} ($n = 5$) for aqueous solution and artificial snow samples, respectively, compared to that of the gas phase were observed in the absorption or excitation spectra. Our data also indicated that there is no significant difference in the spectra bands' maxima between aqueous solutions and snow samples. Moreover, the vibrational analysis of the spectra showed that the identity of the bands remained the same regardless of the phase, which allowed us to assign the individual vibrational bands to specific transitions (Table 1). Comparisons of the vibrational progressions of the *A* and *K* series, corresponding to the harmonic frequency of the first mode in the 1^1B_{2u} state, are shown in Table 5. These values are in accord with the previously reported value of 923 cm^{-1} found for gas-phase benzene.[87]

dx.doi.org/10.1021/jp501094n | J. Phys. Chem. A 2014, 118, 7535−7547

Table 5. Vibrational Progressions of the *A* and *K* Series[a]

experimental conditions		band notation	$\tilde{\nu} \pm$ sd/cm^{-1}	no. vibronic bands considered
aq solution	absorbance; 298 K	*A*	928 ± 12	4
		K	1005 ± 85	4
artificial snow	DR (SF); 253 K	*A*	872 ± 72	6
	DR (VD); 253 K	*A*	913 ± 126	6
	fluorescence (SF); 253 K	*A*	914 ± 66	8
		K	1019 ± 98	4
benzene crystals	DR; 253 K	*A*	880 ± 55	7

[a]See footnotes in Table 1.

Our simulations of the $S_0 \rightarrow S_1$ transition predicted a bathochromic shift of 379 cm^{-1} for the solvated benzene monomer when compared to the spectrum of gas-phase benzene, and a hypsochromic spectral shift of 130 cm^{-1} for benzene on the ice surface in comparison with gas-phase benzene. These predicted energy differences are very small; in fact, they are on the edge of accuracy of the computational methods applied. In the former case, the predicted bathochromic shift is somewhat smaller than the experimental value of (147 ± 11) cm^{-1}. In the latter case, no such hypsochromic shift was found experimentally. A negligible discrepancy might be related to an insufficient size of the ice cluster considered for ice relaxation.

The largest change observed between the gas-phase and condensed-phase spectra of benzene is an appearance of the new *K* series of absorption bands and amplification of the hot 6_1^0 band. The minor *K* series was successfully resolved by derivative analysis of the benzene spectrum in aqueous solution[84] and was also observed in the absorption and excitation spectra of benzene in artificial snow.

The diffuse reflectance spectra of benzene crystals at 253 K showed a 1 nm bathochromically shifted *A* vibrational progression and a well-resolved and wide 6_1^0 band that reached up to 275 nm. Such a shifted absorption was practically nonexistent in aqueous solution or snow in our experiments. All these data, also visualized by a 3D fluorescence plot (Figure 3), unambiguously supported our finding that benzene absorption is limited to wavelengths below 269 nm.

This lack of any substantial bathochromic shift in the absorption spectrum does not support earlier observations of Donaldson and co-workers, who have reported that the absorption bands of aromatic compounds at the air−ice interface exhibit significant bathochromic shifts (up to 320 nm in the case of ice samples prepared by freezing aqueous benzene solutions).[14] Their interpretation was based on a presumption that benzene is self-associated at the air−ice interface into the aggregates. Their spectrum of frozen benzene was considerably different from those published before.[83,84,104]

Our fluorescence emission spectra of benzene (Figure 2) possessed vibrational progressions that are in agreement with those found in the literature.[83,89−91,104] The first mode of the vibrational progression in the ground state was clearly apparent in the emission spectrum. This vibrational mode dominates in the emission of gas-phase benzene,[105] as well as in neat benzene or benzene in an ice matrix, both at 20 K.[104] This is in contrast with the reported data by Donaldson and co-workers, who presented an emission spectrum possessing multiple unassigned bands, which are characteristic neither for benzene nor its excimers.[14]

The emission spectra of benzene dimers and excimers have already been obtained under conditions of supersonic beam expansion (low vibrational excitation).[106] The excimer fluorescence was characterized by a broad peak spanning from 286 to 333 nm with a maximum at 304 nm. This means that the 0−0 energy of an absorbing species must be located below its blue spectral edge (286 nm), which is an upper limit of the absorption spectrum of a hypothetical ground-state dimer. A similar broad featureless band of the benzene excimer has also been observed in concentrated solutions of benzene in nonpolar solvents in the range 320−340 nm.[91] Therefore, our fluorescence emission spectra of benzene in artificial snow (Figure 2) are similar to those obtained under supersonic beam expansion conditions[106] but different from those of liquid nonpolar solutions. Slightly increased emission intensity in the range 290−340 nm thus may indicate the presence of an excimer; however, our attempts at signal quantification were not conclusive.

In our MD simulations, the molecules were typically found lying flat on the ice surface interacting laterally with each other. Structures that resemble the T-shape or tilted T-shape associates were also formed, although less frequently. No structures with sandwich arrangements of the monomers were found even during the subsequent DFT ground-state optimizations of benzene associates−water clusters. It cannot, however, be excluded that the T-shape-like structures would not relax into the excited-state stacked associates after light absorption in a similar way as discussed in our previous studies on 1-methylnaphthalene.[17] For an interpretation of the emission spectra in the region above 290 nm, the emission energies of the T-shape-like associate, as well as the gas-phase optimized benzene excimer and its perturbed dimers, were compared. The emission band of the former structure was unchanged with respect to that of monomer, and thus, it should not be distinguishable from the spectrum of monomer. Our calculation also showed that the interaction of benzene dimers with the ice surface does not affect the absorption spectrum when compared to that of benzene in the gas phase (Table 3).

These findings are thus in agreement with our observation that the excitation spectra do not change at different detection wavelengths (Figure S6). Thus, either dimers are not present or the absorption spectrum of a dimer is quite similar to that of the monomer and cannot be distinguished. It can also be seen from the spectra shown in Figure S6 that a bathochromic shift of neither the $S_0 \rightarrow S_2$ transition of the monomer nor the $S_0 \rightarrow (S_3^d, S_4^d)$ transition of the dimer on the ice surface occurred, which is in accord with our computational simulations. Dimers were previously identified in the excitation spectrum approximately 50 cm^{-1} apart from the 0−0, 6_0^1, and $6_0^1 1_0^1$ vibrations of the benzene monomer.[106] Unfortunately such a resolution that would reveal the presence of benzene dimers on the ice spheres is not achievable in our experiments. Therefore, we cannot decide whether the observed major emission bands are related to monomers or dimers that give essentially the same emission as a monomer.

We also calculated that the excimer should be manifested by an emission band around 320 nm, which agrees with the reported experimental data.[52,91] The formation of such a structure might, however, be restricted by the presence of a relatively rigid structure of the ice surface, and some perturbed variants could be formed. As our calculations revealed, extension of the intermolecular displacement in the face-to-face dimers, as well as slide displacement of the two monomers,

dx.doi.org/10.1021/jp501094n | J. Phys. Chem. A 2014, 118, 7535−7547

lead to a significant decrease of the emission wavelength which could be responsible for features in the measured emission spectra in the region above 290 nm. This could be the reason for hypsochromic shifts in the excimer emission found in the case of the ice surface when compared to the benzene spectra in nonpolar solvents.

CONCLUSIONS

Our spectroscopic analyses of benzene in aqueous solution and at the air−ice interface, supported by our MD/QM calculations, clearly demonstrated that the energy of the $S_0 \rightarrow S_1$ electronic transition is hardly affected by the water microenvironment. Neither of the following phenomena, benzene interactions with ice, the presence of benzene dimers, their interactions with ice, or the presence of benzene microcrystals, should cause any significant bathochromic shift in the absorption spectra. A detailed analysis of the vibrational structure of the $S_0 \rightarrow S_1$ transition allowed us to identify the individual bands and assign them to the previously described transitions. We found that the band energies are not or only very weakly affected by the phase change (the shifts were less than 2 nm). The vibrational band experimentally observed at the longest wavelength is the hot 6_1^0 band with a maximum at 268 nm, and it may be broadened to 275 nm in the case of benzene crystal. Our spectral analysis did not prove or disprove the formation of aggregates on the ice surface, although the probability of their formation[17,18,21,25,107] was very high at higher benzene concentrations. This is also in accord with the theoretical and experimental findings,[61,102,106] according to which the aggregates (dimers) have the absorption spectrum nearly identical with that of monomers. We conclude that the absorption characteristics of benzene monomer and benzene associates on the ice surface are practically the same as those in aqueous solutions.

ASSOCIATED CONTENT

Supporting Information

The absorption and emission spectra; the absorption and emission maxima; and the literature data. This material is available free of charge via the Internet at http://pubs.acs.org.

AUTHOR INFORMATION

Corresponding Authors

*E-mail: dana.nachtigallova@uochb.cas.cz.
*E-mail: hegerd@chemi.muni.cz.
*E-mail: klan@sci.muni.cz.

Notes

The authors declare no competing financial interest.

ACKNOWLEDGMENTS

The project was supported by the Grant Agency of the Czech Republic (P503/10/0947), the Czech Ministry of Education (LO1214) (P.K., D.H.), and the project "Employment of Best Young Scientists for International Cooperation Empowerment" (CZ.1.07/2.3.00/30.0037) cofinanced from the European Social Fund and the state budget of the Czech Republic (R.K.). D.N. acknowledges the funding of the Grant Agency of the Czech Republic (P208/12/1318) and the Czech Ministry of Education, Youth and Sport (LH11021). M.R. acknowledges the support from the Grant Agency of the Czech Republic (P208/10/1724) and the AirUCI Institute funded by the U.S. National Science Foundation (Grant No. 0909227). The research at IOCB was a part of the project RVO:61388963. The authors express their thanks to Jakob Wirz for fruitful discussions.

REFERENCES

(1) Bartels-Rausch, T.; Domine, F.; Jacobi, H. W.; Kahan, T. F.; Thomas, J. L. T. E. S.; Abbatt, J. P. D.; Ammann, M.; Blackford, J. R.; Bluhm, H.; Boxe, C. S.; Frey, M. M.; Gladich, I.; Guzman, M. I.; Heger, D.; Huthwelker, T.; Klan, P.; Kuhs, W. F.; Kuo, M. H.; Maus, S.; Moussa, S. G.; McNeill, V. F.; Newberg, J. T.; Pettersson, J. B. C.; Roeselova, M.; R, S. J. Relationship between Snow Microstructure and Physical and Chemical Processes. *Atmos. Chem. Phys. Discuss.* **2012**, *12*, 30409−30541.

(2) McNeill, V. F.; Grannas, A. M.; Abbatt, J. P. D.; Ammann, M.; Ariya, P.; Bartels-Rausch, T.; Domine, F.; Donaldson, D. J.; Guzman, M. I.; Heger, D.; Kahan, T. F.; Klan, P.; Masclin, S.; Toubin, C.; Voisin, D. Organics in Environmental Ices: Sources, Chemistry, and Impacts. *Atmos. Chem. Phys.* **2012**, *12*, 9653−9678.

(3) Devlin, J. P.; Buch, V. Surface of Ice as Viewed from Combined Spectroscopic and Computer Modeling Studies. *J. Phys. Chem.* **1995**, *99*, 16534−16548.

(4) Devlin, J. P. Molecular Interactions with Icy Surfaces - Infrared Spectra of CO Absorbed in Microporous Amorphous Ice. *J. Phys. Chem.* **1992**, *96*, 6185−6188.

(5) Banham, S. F.; Sodeau, J. R.; Horn, A. B.; McCoustra, M. R. S.; Chesters, M. A. Adsorption and Ionization of HCl on an Ice Surface. *J. Vac. Sci. Technol. A-Vac. Surf. Films* **1996**, *14*, 1620−1626.

(6) Horn, A. B.; Chesters, M. A.; McCoustra, M. R. S.; Sodeau, J. R. Adsorption of Stratospherically Important Molecules on Thin D_2O Ice Films Using Reflection Absorption Infrared Spectroscopy. *J. Chem. Soc., Faraday Trans.* **1992**, *88*, 1077−1078.

(7) Schaff, J. E.; Roberts, J. T. Interaction of Acetonitrile with the Surfaces of Amorphous and Crystalline Ice. *Langmuir* **1999**, *15*, 7232−7237.

(8) Schaff, J. E.; Roberts, J. T. The Adsorption of Acetone on Thin Films of Amorphous and Crystalline Ice. *Langmuir* **1998**, *14*, 1478−1486.

(9) Bartels-Rausch, T.; Huthwelker, T.; Gaggeler, H. W.; Ammann, M. Atmospheric Pressure Coated-Wall Flow-Tube Study of Acetone Adsorption on Ice. *J. Phys. Chem. A* **2005**, *109*, 4531−4539.

(10) Bartels-Rausch, T.; Guimbaud, C.; Gaggeler, H. W.; Ammann, M. The Partitioning of Acetone to Different Types of Ice and Snow between 198 and 223 K. *Geophys. Res. Lett.* **2004**, *31*, art. no L16110.

(11) Borodin, A.; Hofft, O.; Kahnert, U.; Kempter, V.; Krischok, S.; Abou-Helal, M. O. The Interface between Benzenes (C_6H_6; C_6H_5Cl; 2-C_6H_4OHCl) and Amorphous Solid Water Studied with Metastable Impact Electron Spectroscopy and Ultraviolet Photoelectron Spectroscopy (HeI and II). *J. Chem. Phys.* **2004**, *120*, 5407−5413.

(12) Hellebust, S.; O'Riordan, B.; Sodeau, J. Cirrus Cloud Mimics in the Laboratory: An Infrared Spectroscopy Study of Thin Films of Mixed Ice of Water with Organic Acids and Ammonia. *J. Chem. Phys.* **2007**, *126*, art. no 084702.

(13) Ardura, D.; Kahan, T. F.; Donaldson, D. J. Self-Association of Naphthalene at the Air−Ice Interface. *J. Phys. Chem. A* **2009**, *113*, 7353−7359.

(14) Kahan, T. F.; Donaldson, D. J. Benzene Photolysis on Ice: Implications for the Fate of Organic Contaminants in the Winter. *Environ. Sci. Technol.* **2010**, *44*, 3819−3824.

(15) Kahan, T. F.; Donaldson, D. J. Photolysis of Polycyclic Aromatic Hydrocarbons on Water and Ice Surfaces. *J. Phys. Chem. A* **2007**, *111*, 1277−1285.

(16) Matykiewiczova, N.; Kurkova, R.; Klanova, J.; Klan, P. Photochemically Induced Nitration and Hydroxylation of Organic Aromatic Compounds in the Presence of Nitrate or Nitrite in Ice. *J. Photochem. Photobiol., A* **2007**, *187*, 24−32.

(17) Heger, D.; Nachtigallová, D.; Surman, F.; Krausko, J.; Magyarová, B.; Brumovský, M.; Rubeš, M.; Gladich, I.; Klán, P. Self-Organization of 1-Methylnaphthalene on the Surface of Artificial Snow

Grains: A Combined Experimental−Computational Approach. *J. Phys. Chem. A* **2011**, *115*, 11412−11422.
(18) Heger, D.; Klan, P. Interactions of Organic Molecules at Grain Boundaries in Ice: A Solvatochromic Analysis. *J. Photochem. Photobiol., A* **2007**, *187*, 275−284.
(19) Abbatt, J. P. D. Interactions of Atmospheric Trace Gases with Ice Surfaces: Adsorption and Reaction. *Chem. Rev.* **2003**, *103*, 4783−4800.
(20) Cho, H.; Shepson, P. B.; Barrie, L. A.; Cowin, J. P.; Zaveri, R. NMR Investigation of the Quasi-Brine Layer in Ice/Brine Mixtures. *J. Chem. Phys. B* **2002**, *106*, 11226−11232.
(21) Heger, D.; Jirkovsky, J.; Klan, P. Aggregation of Methylene Blue in Frozen Aqueous Solutions Studied by Absorption Spectroscopy. *J. Phys. Chem. A* **2005**, *109*, 6702−6709.
(22) Roth, C. M.; Goss, K. U.; Schwarzenbach, R. P. Sorption of Diverse Organic Vapors to Snow. *Environ. Sci. Technol.* **2004**, *38*, 4078−4084.
(23) Grannas, A. M.; Jones, A. E.; Dibb, J.; Ammann, M.; Anastasio, C.; Beine, H. J.; Bergin, M.; Bottenheim, J.; Boxe, C. S.; Carver, G.; Chen, G.; Crawford, J. H.; Domine, F.; Frey, M. M.; Guzman, M. I.; Heard, D. E.; Helmig, D.; Hoffmann, M. R.; Honrath, R. E.; Huey, L. G.; Hutterli, M.; Jacobi, H. W.; Klan, P.; Lefer, B.; McConnell, J.; Plane, J.; Sander, R.; Savarino, J.; Shepson, P. B.; Simpson, W. R.; Sodeau, J. R.; von Glasow, R.; Weller, R.; Wolff, E. W.; Zhu, T. An Overview of Snow Photochemistry: Evidence, Mechanisms and Impacts. *Atmos. Chem. Phys.* **2007**, *7*, 4329−4373.
(24) Klan, P.; Holoubek, I. Ice (Photo)chemistry. Ice as a Medium for Long-Term (Photo)chemical Transformations - Environmental Implications. *Chemosphere* **2002**, *46*, 1201−1210.
(25) Kurkova, R.; Ray, D.; Nachtigallova, D.; Klan, P. Chemistry of Small Organic Molecules on Snow Grains: The Applicability of Artificial Snow for Environmental Studies. *Environ. Sci. Technol.* **2011**, *45*, 3430−3436.
(26) Matykiewiczova, N.; Klanova, J.; Klan, P. Photochemical Degradation of PCBs in Snow. *Environ. Sci. Technol.* **2007**, *41*, 8308−8314.
(27) Ray, D.; Kurková, R.; Hovorková, I.; Klán, P. Determination of the Specific Surface Area of Snow Using Ozonation of 1,1-Diphenylethylene. *Environ. Sci. Technol.* **2011**, *45*, 10061−10067.
(28) Ray, D.; Malongwe, J. K. E.; Klán, P. Rate Acceleration of the Heterogeneous Reaction of Ozone with a Model Alkene at the Air−Ice Interface at Low Temperatures. *Environ. Sci. Technol.* **2013**, *47*, 6773−6780.
(29) Sander, R.; Bottenheim, J. A Compilation of Tropospheric Measurements of Gas-Phase and Aerosol Chemistry in Polar Regions. *Earth Syst. Sci. Data* **2012**, *4*, 215−282.
(30) Grannas, A. M.; Bogdal, C.; Hageman, K. J.; Halsall, C.; Harner, T.; Hung, H.; Kallenborn, R.; Klan, P.; Klanova, J.; Macdonald, R. W.; Meyer, T.; Wania, F. The Role of the Global Cryosphere in the Fate of Organic Contaminants. *Atmos. Chem. Phys.* **2013**, *13*, 3271−3305.
(31) Jaffrezo, J. L.; Clain, M. P.; Masclet, P. Polycyclic Aromatic Hydrocarbons in the Polar Ice of Greenland. Geochemical Use of these Atmospheric Tracers. *Atmos. Environ.* **1994**, *28*, 1139−1145.
(32) Doskey, P. V.; Gaffney, J. S. Non-Methane Hydrocarbons in the Arctic Atmosphere at Barrow, Alaska. *Geophys. Res. Lett.* **1992**, *19*, 381−384.
(33) Zwier, T. S. The Spectroscopy of Solvation in Hydrogen-Bonded Aromatic Clusters. *Annu. Rev. Phys. Chem.* **1996**, *47*, 205−241.
(34) Fredericks, S. Y.; Jordan, K. D.; Zwier, T. S. Theoretical Characterization of the Structures and Vibrational Spectra of Benzene-$(H_2O)_n$ (n = 1−3) Clusters. *J. Phys. Chem.* **1996**, *100*, 7810−7821.
(35) Gotch, A. J.; Zwier, T. S. Multiphoton Ionization Studies of C_6H_6−$(CH_3OH)_n$ Clusters. II. Intracluster Ion−Molecule Reactions. *J. Chem. Phys.* **1992**, *96*, 3388−3401.
(36) Gruenloh, C. J.; Carney, J. R.; Arrington, C. A.; Zwier, T. S.; Fredericks, S. Y.; Jordan, K. D. Infrared Spectrum of a Molecular Ice Cube: The S-4 and D-2d Water Octamers in Benzene-water$_8$. *Science* **1997**, *276*, 1678−1681.
(37) Kim, K.; Jordan, K. D.; Zwier, T. S. Low-Energy Structures and Vibrational Frequencies of the Water Hexamer: Comparison with Benzene-H_2O_6. *J. Am. Chem. Soc.* **1994**, *116*, 11568−11569.
(38) Pribble, R. N.; Garrett, A. W.; Haber, K.; Zwier, T. S. Resonant Ion-Dip Infrared Spectroscopy of Benzene−H_2O and Benzene−HOD. *J. Chem. Phys.* **1995**, *103*, 531−544.
(39) Pribble, R. N.; Zwier, T. S. Size-Specific Infrared Spectra of Benzene-H_2O_n Clusters (n = 1 through 7): Evidence for Noncyclic H_2O_n Structures. *Science* **1994**, *265*, 75−79.
(40) Pribble, R. N.; Zwier, T. S. Probing Hydrogen Bonding in Benzene−H_2O_n Clusters Using Resonant Ion−Dip IR Spectroscopy. *Faraday Discuss.* **1994**, *97*, 229−241.
(41) Tsai, C. J.; Jordan, K. D. Monte Carlo Simulation of H_2O_8: Evidence for a Low-Energy S4 Structure and Characterization of the Solid Liquid Transition. *J. Chem. Phys.* **1991**, *95*, 3850−3853.
(42) Bahr, S.; Kempter, V. Interaction of Benzene with Amorphous Solid Water Adsorbed on Polycrystalline Ag. *J. Chem. Phys.* **2007**, *127*, art. no 074707.
(43) Silva, S. C.; Devlin, J. P. Interaction of Acetylene, Ethylene, and Benzene with Ice Surfaces. *J. Phys. Chem.* **1994**, *98*, 10847−10852.
(44) Liyana-Arachchi, T. P.; Valsaraj, K. T.; Hung, F. R. Adsorption of Naphthalene and Ozone on Atmospheric Air/Ice Interfaces Coated with Surfactants: A Molecular Simulation Study. *J. Phys. Chem. A* **2012**, *116*, 2519−2528.
(45) Liyana-Arachchi, T. P.; Valsaraj, K. T.; Hung, F. R. Molecular Simulation Study of the Adsorption of Naphthalene and Ozone on Atmospheric Air/Ice Interfaces. *J. Phys. Chem. A* **2011**, *115*, 9226−9236.
(46) Meszar, Z. E.; Hantal, G.; Picaud, S.; Jedlovszky, P. Adsorption of Aromatic Hydrocarbon Molecules at the Surface of Ice, As Seen by Grand Canonical Monte Carlo Simulation. *J. Phys. Chem. C* **2013**, *117*, 6719−6729.
(47) Vacha, R.; Cwiklik, L.; Rezac, J.; Hobza, P.; Jungwirth, P.; Valsaraj, K.; Bahr, S.; Kempter, V. Adsorption of Aromatic Hydrocarbons and Ozone at Environmental Aqueous Surfaces. *J. Phys. Chem. A* **2008**, *112*, 4942−4950.
(48) Amicangelo, J. C. Theoretical Study of the Benzene Excimer Using Time-Dependent Density Functional Theory. *J. Phys. Chem. A* **2005**, *109*, 9174−9182.
(49) Diri, K.; Krylov, A. I. Electronic States of the Benzene Dimer: A Simple Case of Complexity. *J. Phys. Chem. A* **2012**, *116*, 653−662.
(50) Fink, R. F.; Pfister, J.; Zhao, H. M.; Engels, B. Assessment of Quantum Chemical Methods and Basis Sets for Excitation Energy Transfer. *Chem. Phys.* **2008**, *346*, 275−285.
(51) Huenerbein, R.; Grimme, S. Time-Dependent Density Functional Study of Excimers and Exciplexes of Organic Molecules. *Chem. Phys.* **2008**, *343*, 362−371.
(52) Kolaski, M.; Arunkumar, C. R.; Kim, K. S. Aromatic Excimers: Ab Initio and TD-DFT Study. *J. Chem. Theory Comput.* **2013**, *9*, 847−856.
(53) Montero-Alejo, A. L.; Fuentes, M. E.; Montero, L. A.; Garcia de la Vega, J. M. Coulomb and Exchange Contributions to Electronic Excitations of Benzene Aggregates. *Chem. Phys. Lett.* **2011**, *502*, 271−276.
(54) Rocha-Rinza, T.; De Vico, L.; Veryazov, V.; Roos, B. O. A Theoretical Study of Singlet Low-Energy Excited States of the Benzene Dimer. *Chem. Phys. Lett.* **2006**, *426*, 268−272.
(55) Rocha-Rinza, T.; Christiansen, O. Linear Response Coupled Cluster Study of the Benzene Excimer. *Chem. Phys. Lett.* **2009**, *482*, 44−49.
(56) Shirai, S.; Iwata, S.; Tani, T.; Inagaki, S. Ab Initio Studies of Aromatic Excimers Using Multiconfiguration Quasi-Degenerate Perturbation Theory. *J. Phys. Chem. A* **2011**, *115*, 7687−7699.
(57) Vala, M. T.; Hillier, I. H.; Rice, S. A.; Jortner, J. Theoretical Studies of Transannular Interactions. I. Benzene Excimer Fluorescence and the Singlet States of the Paracyclophanes. *J. Chem. Phys.* **1966**, *44*, 23−35.
(58) Forster, T. Excimers. *Angew. Chem., Int. Ed.* **1969**, *8*, 333−343.

(59) Grimme, S. Semiempirical GGA-Type Density Functional Constructed with a Long-Range Dispersion Correction. *J. Comput. Chem.* **2006**, *27*, 1787−1799.
(60) Schafer, A.; Huber, C.; Ahlrichs, R. Fully Optimized Contracted Gaussian Basis Sets of Triple Zeta Valence Quality for Atoms Li to Kr. *J. Chem. Phys.* **1994**, *100*, 5829−5835.
(61) Rubes, M.; Bludsky, O.; Nachtigall, P. Investigation of the Benzene-Naphthalene and Naphthalene-Naphthalene Potential Energy Surfaces: DFT/CCSD(T) Correction Scheme. *ChemPhysChem* **2008**, *9*, 1702−1708.
(62) Schirmer, J. Beyond the Random-Phase Approximation: A New Approximation Scheme for the Polarization Propagator. *Phys. Rev. A* **1982**, *26*, 2395−2416.
(63) Trofimov, A. B.; Schirmer, J. An Efficient Polarization Propagator Approach to Valence Electron Excitation Spectra. *J. Phys. B-At. Mol. Opt.* **1995**, *28*, 2299−2324.
(64) Hattig, C. Structure Optimizations for Excited States with Correlated Second-Order Methods: CC2 and ADC(2). In *Advances in Quantum Chemistry, Vol 50: A Tribute to Jan Linderberg and Poul Jorgensen*; Sabin, J. R., Brandas, E., Eds.; **2005**; Vol. *50*, pp 37−60.
(65) Stratmann, R. E.; Scuseria, G. E.; Frisch, M. J. An Efficient Implementation of Time-Dependent Density-Functional Theory for the Calculation of Excitation Energies of Large Molecules. *J. Chem. Phys.* **1998**, *109*, 8218−8224.
(66) Bauernschmitt, R.; Ahlrichs, R. Treatment of Electronic Excitations within the Adiabatic Approximation of Time Dependent Density Functional Theory. *Chem. Phys. Lett.* **1996**, *256*, 454−464.
(67) Becke, A. D. Density Functional Thermochemistry. III. The Role of Exact Exchange. *J. Chem. Phys.* **1993**, *98*, 5648−5652.
(68) Hellweg, A.; Grün, S. A.; Hättig, C. Benchmarking the Performance of Spin-Component Scaled CC2 in Ground and Electronically Excited States. *Phys. Chem. Chem. Phys.* **2008**, *10*, 4119−4127.
(69) Frisch, M. J.; Trucks, G. W.; Schlegel, H. B.; Scuseria, G. E.; Robb, M. A.; Cheeseman, J. R.; Scalmani, G.; Barone, V.; Mennucci, B.; Petersson, G. A.; Nakatsuji, H.; Caricato, M.; Li, X.; Hratchian, H. P.; Izmaylov, A. F.; Bloino, J.; Zheng, G.; Sonnenberg, J. L.; Hada, M.; Ehara, M.; Toyota, K.; Fukuda, R.; Hasegawa, J.; Ishida, M.; Nakajima, T.; Honda, Y.; Kitao, O.; Nakai, H.; Vreven, T.; Montgomery, J. J. A. ; Peralta, J. E.; Ogliaro, F.; Bearpark, M.; Heyd, J. J.; Brothers, E.; ; Kudin, K. N.; Staroverov, V. N.; Kobayashi, R.; Normand, J.; Raghavachari, K.; Rendell, A.; Burant, J. C.; Iyengar, S. S.; Tomasi, J.; Cossi, M.; Rega, N.; Millam, J. M.; Klene, M.; Knox, J. E.; Cross, J. B.; Bakken, V.; Adamo, C.; Jaramillo, J.; Gomperts, R.; Stratmann, R. E.; Yazyev, O.; Austin, A. J.; Cammi, R.; Pomelli, C.; Ochterski, J. W.; Martin, R. L.; Morokuma, K.; Zakrzewski, V. G.; Voth, G. A.; Salvador, P.; Dannenberg, J. J.; Dapprich, S.; Daniels, A. D.; Farkas, Ö.; Foresman, J. B.; Ortiz, J. V.; Cioslowski, J.; Fox, D. J. *Gaussian 09*, Revision A.1; Gaussian, Inc.: Wallingford, CT, 2009.
(70) Ahlrichs, R.; Bar, M.; Haser, M.; Horn, H.; Kolmel, C. Electronic Structure Calculations on Workstation Computers: The Program System Turbomole. *Chem. Phys. Lett.* **1989**, *162*, 165−169.
(71) Rick, S. W. A Reoptimization of the Five-Site Water Potential (TIP5P) for Use with Ewald Sums. *J. Chem. Phys.* **2004**, *120*, 6085−6093.
(72) Oostenbrink, C.; Villa, A.; Mark, A. E.; Van Gunsteren, W. F. A Biomolecular Force Field Based on the Free Enthalpy of Hydration and Solvation: The GROMOS Force-Field Parameter Sets 53A5 and 53A6. *J. Comput. Chem.* **2004**, *25*, 1656−1676.
(73) Buch, V.; Sandler, P.; Sadlej, J. Simulations of H_2O Solid, Liquid, and Clusters, with an Emphasis on Ferroelectric Ordering Transition in Hexagonal Ice. *J. Chem. Phys. B* **1998**, *102*, 8641−8653.
(74) Bernal, J. D.; Fowler, R. H. A Theory of Water and Ionic Solution, with Particular Reference to Hydrogen and Hydroxyl Ions. *J. Chem. Phys.* **1933**, *1*, 515−548.
(75) Parrinello, M.; Rahman, A. Polymorphic Transitions in Single-Crystals - a New Molecular-Dynamics Method. *J. Appl. Phys.* **1981**, *52*, 7182−7190.
(76) Vega, C.; Martin-Conde, M.; Patrykiejew, A. Absence of Superheating for Ice I_h with a Free Surface: A New Method of Determining the Melting Point of Different Water Models. *Mol. Phys.* **2006**, *104*, 3583−3592.
(77) Hess, B.; Kutzner, C.; van der Spoel, D.; Lindahl, E. GROMACS 4: Algorithms for Highly Efficient, Load-Balanced, and Scalable Molecular Simulation. *J. Chem. Theory Comput.* **2008**, *4*, 435−447.
(78) Hockney, R. W.; Goel, S. P.; Eastwood, J. W. Quiet High-Resolution Computer Models of a Plasma. *J. Comput. Phys.* **1974**, *14*, 148−158.
(79) Darden, T.; York, D.; Pedersen, L. Particle Mesh Ewald - an N.Log(N) Method for Ewald Sums in Large Systems. *J. Chem. Phys.* **1993**, *98*, 10089−10092.
(80) Essmann, U.; Perera, L.; Berkowitz, M. L.; Darden, T.; Lee, H.; Pedersen, L. G. A Smooth Particle Mesh Ewald Method. *J. Chem. Phys.* **1995**, *103*, 8577−8593.
(81) Hess, B.; Bekker, H.; Berendsen, H. J. C.; Fraaije, J. LINCS: A Linear Constraint Solver for Molecular Simulations. *J. Comput. Chem.* **1997**, *18*, 1463−1472.
(82) Miyamoto, S.; Kollman, P. A. SETTLE - an Analytical Version of the Shake and Rattle Algorithm for Rigid Water Models. *J. Comput. Chem.* **1992**, *13*, 952−962.
(83) Schwarz, F. P.; Wasik, S. P. Fluorescence Measurements of Benzene, Naphthalene, Anthracene, Pyrene, Fluoranthene, and Benzo[e]pyrene in Water. *Anal. Chem.* **1976**, *48*, 524−528.
(84) Inagaki, T. Absorption Spectra of Pure Liquid Benzene in the Ultraviolet Region. *J. Chem. Phys.* **1972**, *57*, 2526−2530.
(85) Cardinal, J. R.; Mukerjee, P. Solvent Effects on the Ultraviolet Spectra of Benzene Derivatives and Naphthalene. Identification of Polarity Sensitive Spectral Characteristics. *J. Phys. Chem.* **1978**, *82*, 1614−1620.
(86) Petrov, V.; Antonov, L.; Ehara, H.; Harada, N. Step by Step Filter Based Program for Calculations of Highly Informative Derivative Curves. *Comput. Chem.* **2000**, *24*, 561−569.
(87) Callomon, J. H.; Dunn, T. M.; Mills, I. M. Rotational Analysis of the 2600 Å Absorption System of Benzene. *Philos. Trans. R. Soc. A* **1966**, *259*, 499−531.
(88) Bernhardsson, A.; Forsberg, N.; Malmqvist, P. A.; Roos, B. O.; Serrano-Andres, L. A Theoretical Study of the $B1_{2u}$ and $B1_{1u}$ Vibronic Bands in Benzene. *J. Chem. Phys.* **2000**, *112*, 2798−2809.
(89) Lumb, M. D.; Braga, C. L.; Pereira, L. C. Emission Spectra and Phosphorescence Lifetime of Benzene Solutions at 77 K as a Function of Concentration and Excitation Wavelength. *Trans. Faraday Soc.* **1969**, *65*, 1992−1999.
(90) Johnston, D. B.; Lipsky, S. A Redetermination of the $^1B_{2u}$-$^1A_{1g}$ Fluorescence Quantum Yield of Benzene Vapor. *J. Phys. Chem.* **1991**, *95*, 3486−3491.
(91) Hirayama, F.; Lipsky, S. Excimer Fluorescence of Benzene and Its Alkyl Derivatives—Concentration and Temperature Dependence. *J. Chem. Phys.* **1969**, *51*, 1939−1951.
(92) Christiansen, O.; Stanton, J. F.; Gauss, J. A Coupled Cluster Study of the 1^1A_{1g} and 1^1B_{2u} States of Benzene. *J. Chem. Phys.* **1998**, *108*, 3987−4001.
(93) Lorentzon, J.; Malmqvist, P. A.; Fulscher, M.; Roos, B. O. A Caspt2 Study of the Valence and Lowest Rydberg Electronic States of Benzene and Phenol. *Theor. Chim. Acta* **1995**, *91*, 91−108.
(94) Schreiber, M.; Silva, M. R. J.; Sauer, S. P. A.; Thiel, W. Benchmarks for Electronically Excited States: CASPT2, CC2, CCSD, and CC3. *J. Chem. Phys.* **2008**, *128*, art. no 134110.
(95) Li, Y.; Wan, J.; Xu, X. Theoretical Study of the Vertical Excited States of Benzene, Pyrimidine, and Pyrazine by the Symmetry Adapted Cluster-Configuration Interaction Method. *J. Comput. Chem.* **2007**, *28*, 1658−1667.
(96) Li, X.; Paldus, J. Multi-Reference State-Universal Coupled-Cluster Approaches to Electronically Excited States. *J. Chem. Phys.* **2011**, *134*, art. no 214118.
(97) Ma, H.; Ma, Y. Solvatochromic Shifts of Polar and Non-polar Molecules in Ambient and Supercritical Water: A Sequential Quantum Mechanics/Molecular Mechanics Study Including Solute-Solvent

Electron Exchange Correlation. *J. Chem. Phys.* **2012**, *137*, art. no 214504.
(98) Bayliss, N. S.; Hulme, L. Solvent Effects in the Spectra of Benzene, Toluene, and Chlorobenzene at 2600 Å and 2000 Å. *Aust. J. Chem.* **1953**, *6*, 257−277.
(99) Hill, J. G.; Platts, J. A.; Werner, H.-J. Calculation of Intermolecular Interactions in the Benzene Dimer Using Coupled-Cluster and Local Electron Correlation Methods. *Phys. Chem. Chem. Phys.* **2006**, *8*, 4072−4078.
(100) Janowski, T.; Pulay, P. High Accuracy Benchmark Calculations on the Benzene Dimer Potential Energy Surface. *Chem. Phys. Lett.* **2007**, *447*, 27−32.
(101) Pitonak, M.; Neogrady, P.; Rezac, J.; Jurecka, P.; Urban, M.; Hobza, P. Benzene Dimer: High-Level Wave Function and Density Functional Theory Calculations. *J. Chem. Theory Comput.* **2008**, *4*, 1829−1834.
(102) Bludsky, O.; Rubes, M.; Soldan, P.; Nachtigall, P. Investigation of the Benzene-Dimer Potential Energy Surface: DFT/CCSD(T) Correction Scheme. *J. Chem. Phys.* **2008**, *128*, art. no 114102.
(103) Coutinho, K.; Canuto, S.; Zerner, M. C. Calculation of the Absorption Spectrum of Benzene in Condensed Phase. A Study of the Solvent Effects. *Int. J. Quantum Chem.* **1997**, *65*, 885−891.
(104) Johnson, P. V.; Hodyss, R.; Bolser, D. K.; Bhartia, R.; Lane, A. L.; Kanik, I. Ultraviolet-Stimulated Fluorescence and Phosphorescence of Aromatic Hydrocarbons in Water Ice. *Astrobiology* **2011**, *11*, 151−156.
(105) Nicholson, J. A.; Lawrance, W. D.; Fischer, G. Single Vibronic Level Fluorescence Spectra from $^1B_{2U}$ Benzene - Fermi Resonances and S-0 IVR Lifetimes. *Chem. Phys.* **1995**, *196*, 327−351.
(106) Hirata, T.; Ikeda, H.; Saigusa, H. Dynamics of Excimer Formation and Relaxation in the T-shaped Benzene Dimer. *J. Phys. Chem. A* **1999**, *103*, 1014−1024.
(107) Klan, P.; Janosek, J.; Kriz, Z. Photochemistry of Valerophenone in Solid Solutions. *J. Photochem. Photobiol., A* **2000**, *134*, 37−44.